

Original Research Article

Inhibitory Activity of Natural Flavonoids against Protein Aggregation in Alzheimer's disease: A Computational Simulation Study

Saba Hadidi^{1*} , Mohammad Hosein Farzaei²

¹ Department of Inorganic Chemistry, Faculty of Chemistry, Razi University, Kermanshah, Iran

² Pharmaceutical Sciences Research Center, Health Institute, Kermanshah University of Medical Sciences, Kermanshah, Iran

ARTICLE INFO

Article history

Submitted: 01 January 2023

Revised: 24 February 2023

Accepted: 26 February 2023

Available online: 01 March 2023

Manuscript ID: [AJCA-2301-1350](#)

Checked for Plagiarism: [Yes](#)

DOI: [10.22034/AJCA.2023.379103.1350](#)

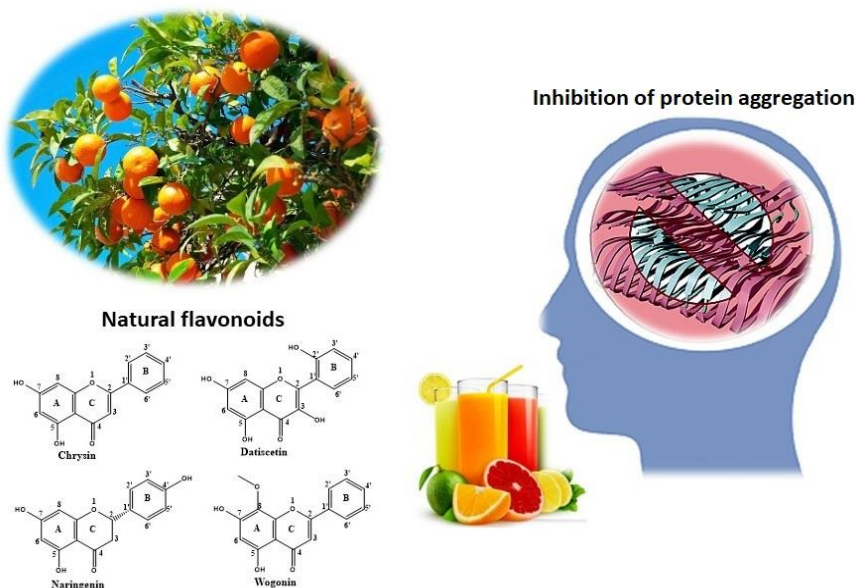
KEYWORDS

Alzheimer's disease
Amyloid-beta peptide
Tau protein
Natural flavonoids
Molecular simulation

ABSTRACT

In this study, the prevention mechanism of chrysin, datiscetin, naringenin, and wogonin against A β peptide and tau protein aggregation was investigated using computational simulation methods. According to the molecular docking data, minor differences in the chemical structures of candidate compounds do not result in significant differences in docking binding energy. Instead, the ligand binding site and residue contact degree appear to have played a more significant role. Naringenin showed the highest affinity for tau protein due to its different binding site. Because of more residue contacts, chrysin and datiscetin also had a higher amyloid binding affinity. The secondary structure analysis of amyloid β revealed a significant loss of α -helix content in all systems studied with the formation of turns and random coils, which is most in the presence of wogonin. In all tau-ligand systems, the percentage of the coil decreased. In contrast, the turn percentage increased, indicating that the selected compounds can prevent the aggregation of AD-related receptors.

GRAPHICAL ABSTRACT



* Corresponding author: Hadidi, Saba

✉ E-mail: s.hadidi@razi.ac.ir

© 2023 by SPC (Sami Publishing Company)

Introduction

Alzheimer disease (AD) is a significant cause of functional disability in older adults, inflicting massive costs and suffering on patients, caregivers, and society [1, 2]. Since age is a crucial risk factor for AD, it is fast becoming a major and growing healthcare problem as the global population ages [3]. Because currently available medicines are only effective in treating the symptoms, new therapeutic approaches to AD are needed [4-7]. If novel treatment strategies are unavailable, the number of AD patients is expected to rise to 130 million in 2050 [8, 9]. Successful treatment of AD requires accurate knowledge of its pathological features [10-14]. It is believed that the accumulation of amyloid-beta ($A\beta_{1-42}$) peptides in the extracellular brain space [15] and tau aggregation or neurofibrillary tangles (NFTs) formation inside the cell may play influential roles in AD pathogenesis [16]. Therefore, inhibiting $A\beta_{1-42}$ peptide and tau aggregation has been considered a promising approach for treating AD [17-19]. There is mounting evidence that some dietary flavonoids can protect against AD by disrupting the production and aggregation of $A\beta_{1-42}$ peptides and reducing tau aggregation [20-22]. For example, through the mTOR/autophagy signaling pathway, wogonin could potentially promote $A\beta$ clearance in the primary neural astrocytes and reduced $A\beta$ secretion in SH-SY5Y-APP and BACE1 cells substantially. Wogonin also inhibited GSK3 β activity via inhibiting mTOR, resulting in a reduction in tau phosphorylation in SH-SY5Y cells and primary neural astrocytes [23]. A study by Ghofrani *et al.* showed that $A\beta$ -induced impairment of learning and memory was reduced in the presence of Naringenin [24]. Other studies by Irie *et al.* [25] provided structural insights into the mechanisms of action for anti- $A\beta_{42}$ aggregation by non-catechol-type flavonoids (morin, datiscetin, and kaempferol).

The aggregation experiments demonstrated that kaempferol and its degradation products inhibited the elongation rather than the nucleation phase, indicating that they interacted with small aggregates of $A\beta_{42}$ but not with the monomer. Morin and datiscetin, on the other hand, inhibited both phases. Based on the findings, non-catechol-type flavonoids' inhibitory potencies and mechanisms against $A\beta_{42}$ aggregation may be influenced by the location and number of hydroxyl groups on the B-ring [25]. By encapsulating chrysin (CN) in solid lipid nanoparticles (SLNs), Vedagiri and Thangarajan showed that the therapeutic effectiveness of chrysin could be achieved at lower doses while simultaneously increasing its oral bioavailability.

Consequently, the findings imply that CN-SLNs might be a viable therapeutic and brain-targeting method to treat Alzheimer's disease's worldwide impact [26]. The high potency and low systemic toxicity of natural flavonoids make them viable alternatives to conventional therapeutic drugs. Efficient development of new drugs based on flavonoids for reducing $A\beta$ or tau aggregation requires detailed information about the mechanism of action of these compounds. However, because this information is difficult to obtain using traditional experimental techniques, theoretical methods are ideal for this field. The information obtained from molecular docking and molecular dynamics simulations will most likely speed up the process of developing new Alzheimer's drugs, and it has already been used successfully in designing $A\beta$ /tau aggregation inhibitors [19, 27-29]. Therefore, in the present study we provided structural insights into the inhibitory potencies and mechanisms of natural flavonoids such as wogonin, naringenin, datiscetin and chrysin against $A\beta_{1-42}$ and tau aggregation using computational techniques.

Materials and methods

Molecular docking simulations

Molecular docking studies were carried out using AutoDock Vina version 1.1.2. The 3D structures of wogonin, naringenin, datiscetin, and chrysin as ligands were obtained in .mol format from the ChemSpider database (<http://www.chemspider.com>) [30]. Crystal structure of the A β ₁₋₄₂ peptide (PDB code: 1IYT) and tau protein (PDB code: 5O3L) were retrieved in .pdb format from RCSB PDB database (<http://www.rcsb.org/pdb>) [31]. The 1IYT has 10 NMR-determined structure models [32]. For calculations, the structure of Model 1, with the most similarity to the other models, was chosen as the A β ₁₋₄₂ peptide monomer. Before docking calculations, the proteins were modified by removing solvent molecules, ions, and unnecessary protein chains. The polar hydrogen atoms and Gasteiger charges were included in the receptor structure, and then the protein in PDBQT format was used as an input for the AutoDock Vina program [33]. All other settings were left at their default value. A three-dimensional grid box with 40×30×50 Å and 76×62×30 Å with a spacing of 1.0 Å was centered at x: -4.108, y: 1.139, z: 0.954 and x: 203.869, y: 150.533, z: 158.733 for A β ₁₋₄₂ peptide and tau protein, respectively. The best energy docked conformation was picked from the 20 lowest energy conformers from the 500 runs for each docking case. The interactions and binding modes of ligands with A β ₁₋₄₂ peptide and tau protein were analyzed using Discovery Studio Visualizer 2021.

Molecular dynamic simulations

MD simulations were performed using the Desmond software package [34, 35] under the NPT ensemble at a temperature of 300 K and a pressure of 1 bar. The water molecules were specifically defined using the simple point charge model [36]. The Nose Hoover chain coupling method was utilized for temperature control, while the Martyna-Tuckerman-Klein chain

coupling scheme with a coupling constant of 2.0 ps was employed for pressure control [37]. During the simulation, the OPLS 2005 force field parameters were utilized [38]. The system was simulated in 50 nanoseconds with bonded, near, and distant time steps of 0.002, 0.002, and 0.006, respectively. The results were evaluated using the VMD-Visual Molecular Dynamics [39] and Maestro Simulation Interaction Diagram tool [40].

Results and discussion

Molecular docking analysis of amyloid β

The molecular structure of selected ligands with the atom numbering used throughout the study is demonstrated in Figure 1.

Based on the docking simulation results for amyloid β , all selected natural flavonoids were able to interact with the A β ₁₋₄₂ peptide by possessing a close binding energy value. Figure 2 presents the binding state of chrysin into A β ₁₋₄₂ peptide with a binding affinity of -5.5 kcal/mol. Figure 2 shows that chrysin is linked to Gln15, Lys16, and Phe19 residues through noncovalent molecular interactions. The oxygen atom of the =CO group in chrysin generates a hydrogen bond with -NH₂ group of the Gln15 amino acid at a distance of 1.96 Å. The aromatic side chain of Phe19 is positioned over the ligand molecule, making two pi-pi stacking interactions with the phenyl rings. The docking pose of chrysin displayed two pi-alkyl interactions between C γ in Lys16 with the center of six-carbon rings. Also, a pi-cation interaction was formed between a positive N atom in Lys19 and the π electron-rich phenyl group in the ligand. According to LC-MS and solid-state NMR studies, catechol-type flavonoids, the *o*-quinone structure obtained from autoxidation formed a Michael adduct with Lys16 and 28 inside the intermolecular β -sheet region in A β ₄₂, inhibiting amyloid beta peptide aggregation [41].

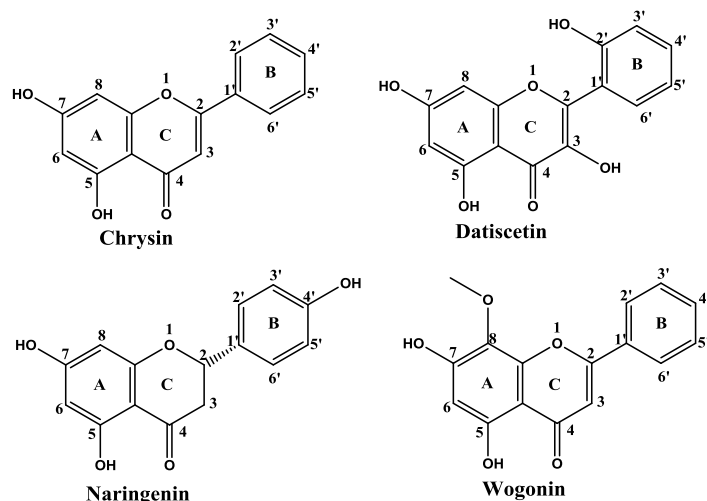


Figure 1. The molecular structure of selected ligands with atom numbering

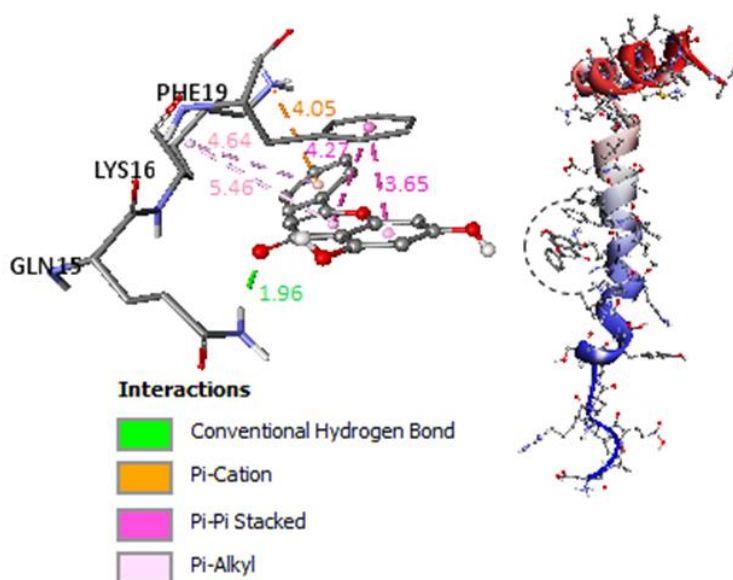


Figure 2. Chrysin docked into $A\beta_{1-42}$ peptide (right) and amino acid residues involved in the interaction (left) the dashed lines show the distance (in Å)

A molecular simulation of the interaction of chrysin derivatives with amyloid β revealed that placing the electron-donating group (dimethylamino) as an active group on the benzene ring increases its binding affinity by about 0.9 kcal/mol [42]. The oxygen atom of pyrone in dimethylamino-chrysin could form a hydrogen bond with Gln15 with a distance of 3.0 Å. And another hydrogen bond was formed between the phenolic hydroxyl group of the A

ring and the Ser8. A carbon-hydrogen interaction was also created between the dimethylamino group with Glu11. Furthermore, dimethylamino-chrysin demonstrated van der Waals interactions with Gly9, His14, and Phe19. This is significant because His14 involves the β -sheet conformation in $A\beta$ aggregation [43]. Thus, it is hypothesized that these interactions between $A\beta$ helix and dimethylamino-chrysin might favor interfering and dissociating the $A\beta$ aggregation.

Datiscetin showed similar binding energy for the A β ₁₋₄₂ peptide (-5.5 kcal/mol). The significant intermolecular hydrogen bonds have been constructed between the H atom of two hydroxyl substituents at positions 2' and 7 with the O atom of the carbonyl group in Glu3 and Gly9 residues with a bond lengths 2.46 and 2.40 Å, respectively (Figure 3).

The one intramolecular hydrogen bond between H of -OH5 and O of the carbonyl group in the ligand molecule reduces the receptor binding efficiency. The hydroxyl group at position 3 did not form a hydrogen bond with

binding residues. The datiscetin-amyloid β conjugate is also stabilized by vertical pi-pi stacking interactions, which form between the aromatic rings of the ligand molecule and surrounding binding site residues (Tyr10 and His6).

The binding interaction of naringenin with A β ₁₋₄₂ peptide was observed with the affinity of -5.4 kcal/mol, less than chrysin and datiscetin. From Figure 4, it can be seen that naringenin interacts with two amino acids through three types of interactions. Two O-H...O type hydrogen bonds

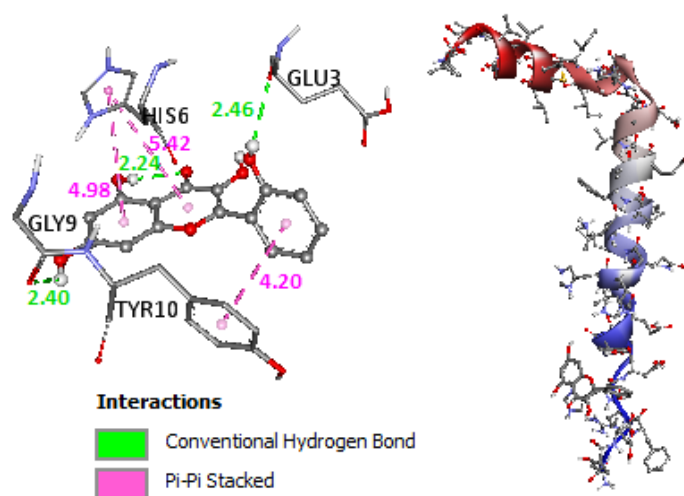


Figure 3. Datiscetin docked into A β ₁₋₄₂ peptide (right) and amino acid residues involved in the interaction (left) the dashed lines show the distance (in Å)

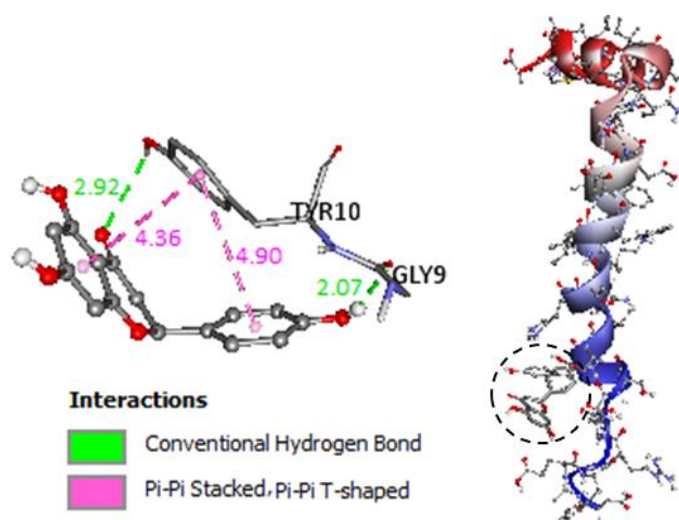


Figure 4. Naringenin docked into A β ₁₋₄₂ peptide (right) and amino acid residues involved in the interaction (left) the dashed lines show the distance (in Å)

between H of the hydroxyl group at position 4' with O of a carbonyl group in Gly9 and =CO group in ligand with -OH group in Tyr10 at distances of 2.07 and 2.92 Å, respectively, a pi-pi stacking and one pi-pi T-shape interactions between aromatic benzene ring in the side chain of Tyr10 with six-carbon ring A and C in naringenin, respectively.

Figure 5 shows the docking pose for wogonin with a binding energy of -5.4 kcal/mol. Three H-bonds are observed in Figure 5, playing crucial roles in anchoring the ligand molecule in the binding site. The -NH₂ of Gln15 as the hydrogen bond donor forms two H-bonds with O atoms of the carbonyl group and -OH5 in wogonin with a distance of 1.95 and 2.33 Å, respectively. Besides

this, the OH5 acts as a donor site, and the O atom of =CO group in Val12 as an acceptor site in the O-H...O hydrogen bond at a distance of 2.71 Å. The only structural difference between chrysin and wogonin is the methoxy substituent at position 8, which can serve for hydrophobic interaction with the surrounding environment (alkyl-type interaction with Val12). The protein-ligand complex was also stabilized by two types of hydrophobic interactions, one pi-sigma interaction between side chains of Val12 and aromatic ring A of wogonin and a pi-alkyl interaction between six-membered carbon ring of the ligand with Cy in Lys16.

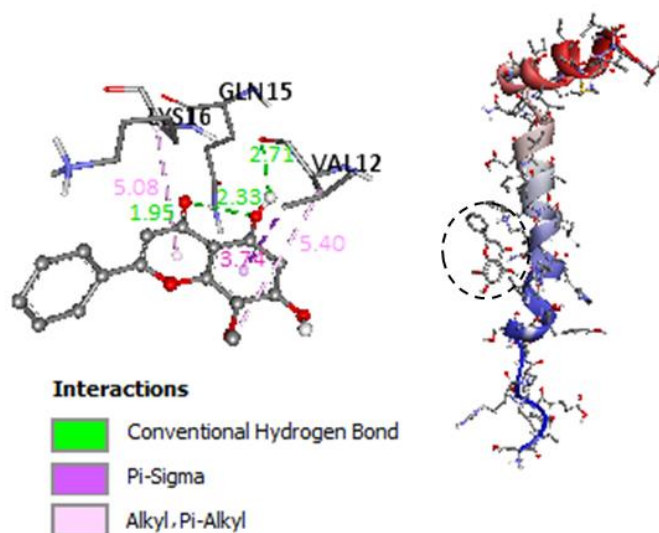


Figure 5. Wogonin docked into A β ₁₋₄₂ peptide (right) and amino acid residues involved in the interaction (left) the dashed lines show the distance (in Å)

Molecular docking analysis of tau protein

The docking outcomes for tau protein and selected candidates revealed that these compounds have also potentially interacted with the residues of the receptor with binding energies ranging from -5.5 to -5.9 kcal/mol. Figure 6 reveals the docking pose of chrysin and the amino acid neighbors. There were four distinct forms of non-covalent interactions as a result of the ligand binding to the receptor with affinity -5.5 kcal/mol. Two pi-alkyl interactions

were formed between rings B and C in the ligand molecule with the Ile328 side chain. The six-membered ring C also participated in a pi-sigma interaction with Val363. Between π electrons of aromatic ring A with Val363 and H of -NH₂ group in His362, a pi-alkyl interaction, and one pi-donor hydrogen bond were observed, respectively. A conventional hydrogen bond stabilized the ligand-receptor complex at a distance of 2.31 Å, which formed between O of =CO group in His362 as the acceptor site and H of the hydroxyl group at position 5 as a donor site.

The carbonyl group of chrysin, -OH7, and the O atom at position 1 did not form any hydrogen bond with tau protein amino acids.

The main interactions of datiscetin with amino acids in tau protein are Val363, Ile328, Leu325, His329, and Ile360, with a binding affinity -5.7 kcal/mol (Figure 7). Hydrogen bonds and hydrophobic interactions maintain the conformational stability of the datiscetin-tau protein complex. Two hydrophobic residues (Val363 and Ile328) can participate in both pi-alkyl and pi-sigma interactions with six-

membered carbon rings of ligand. However, only one form of association was found for each of the three amino acids Leu325, His329, and Ile360, a pi-alkyl interaction between aromatic ring B and Leu325, and two hydrogen bonds between H atoms of -OH group at positions 5 and 7 with O atoms of carbonyl groups in His329 and Ile360, respectively. The donor (-OH3) and acceptor (=CO) groups in datiscetin could not form hydrogen bonds at the ligand-receptor binding site.

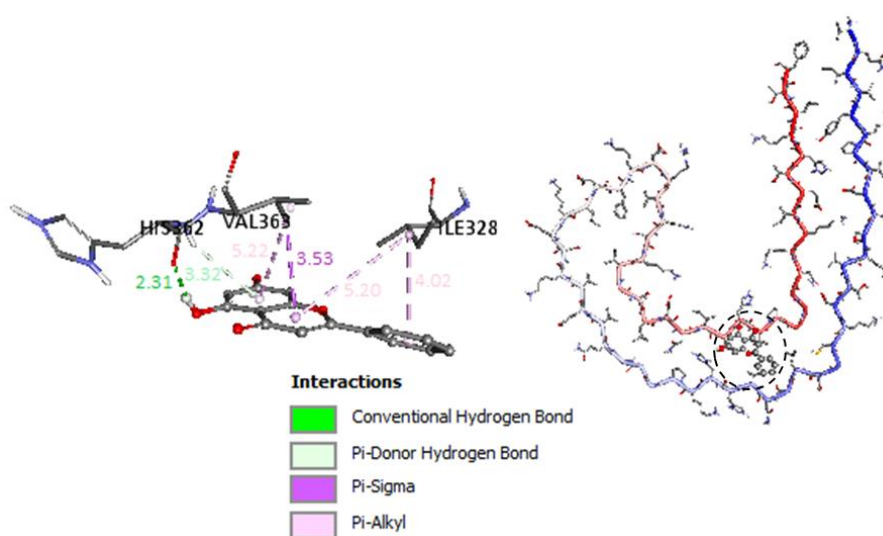


Figure 6. Chrysin docked into tau protein (right) and amino acid residues involved in the interaction (left) the dashed lines show the distance (in Å)

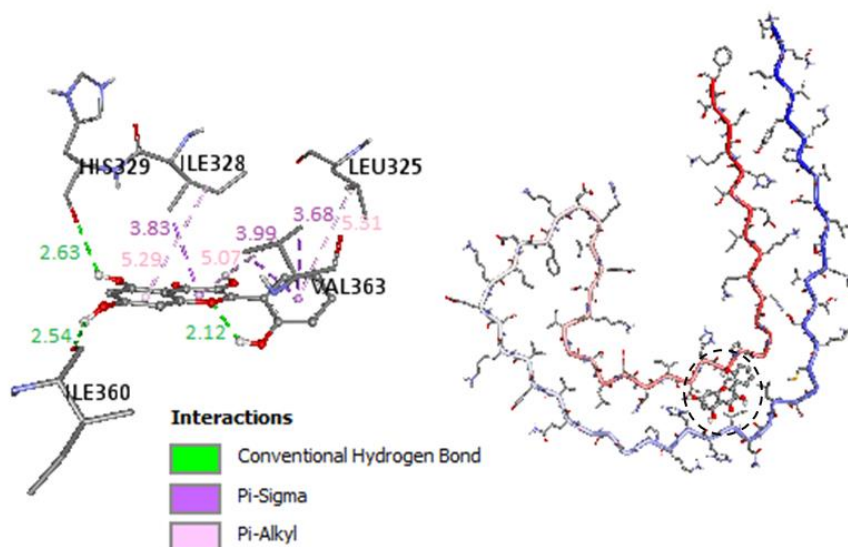


Figure 7. Datiscetin docked into tau protein (right) and amino acid residues involved in the interaction (left) the dashed lines show the distance (in Å)

The highest binding affinity (-5.9 kcal/mol) was obtained for naringenin, which binds to tau protein in a different position than chrysin and datiscetin, as shown in Figure 8. Both types of H-acceptor (O of =CO with H of -OH in Phe364) and H-donor (H of -OH5 with O of Leu344) interactions were observed between ligands atoms and amino acids that play crucial roles in anchoring the ligand in the binding site. A pi-pi stacking and a pi-alkyl interaction were formed between Phe346 and Val350 side chains with the center of aromatic rings A and B, respectively. An unfavorable donor-donor interaction and one intramolecular H-bond were observed between -OH4' with -NH₂ of Val350 and -OH5 with =CO group in naringenin, respectively.

Wogonin interacts with tau protein similarly to chrysin and datiscetin, with a slight difference in binding energy (-5.6 kcal/mol). Key residues involved in receptor binding are shown in Figure 9. Hydrophobic-type interactions, including alky, pi-alkyl, and pi-sigma, were observed in the binding of ligands to Ile328, Val363, and Leu325 amino acids. A pi-donor and a conventional hydrogen bond were formed between the carbonyl and -NH₂ group of His329 with -OH at position 5 and aromatic ring A of wogonin, respectively. The methoxy group, located at position 8 in aromatic ring A, plays a critical role in forming a carbon-hydrogen bond with =CO group in His329.

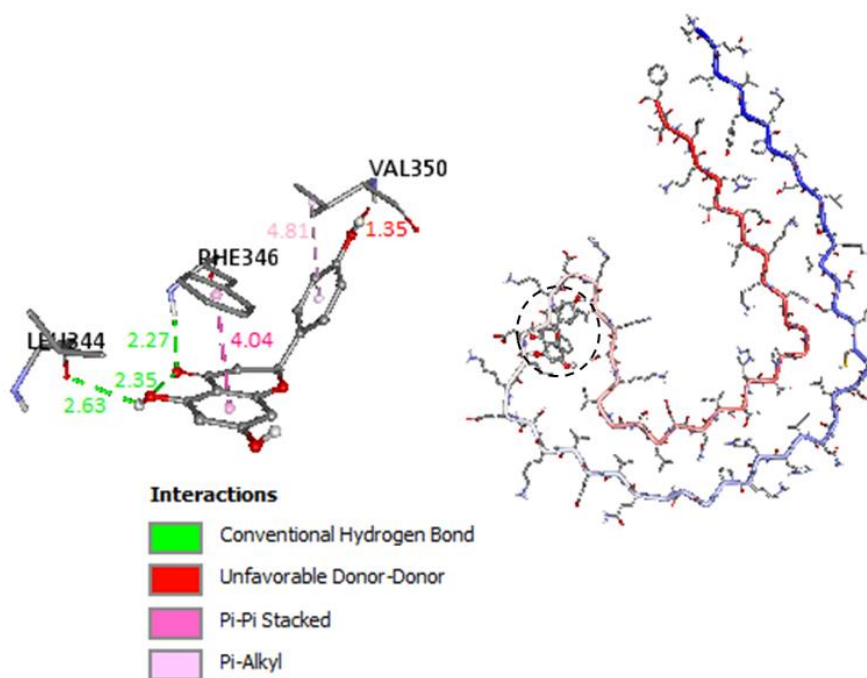


Figure 8. Naringenin docked into tau protein (right) and amino acid residues involved in the interaction (left) the dashed lines show the distance (in Å)

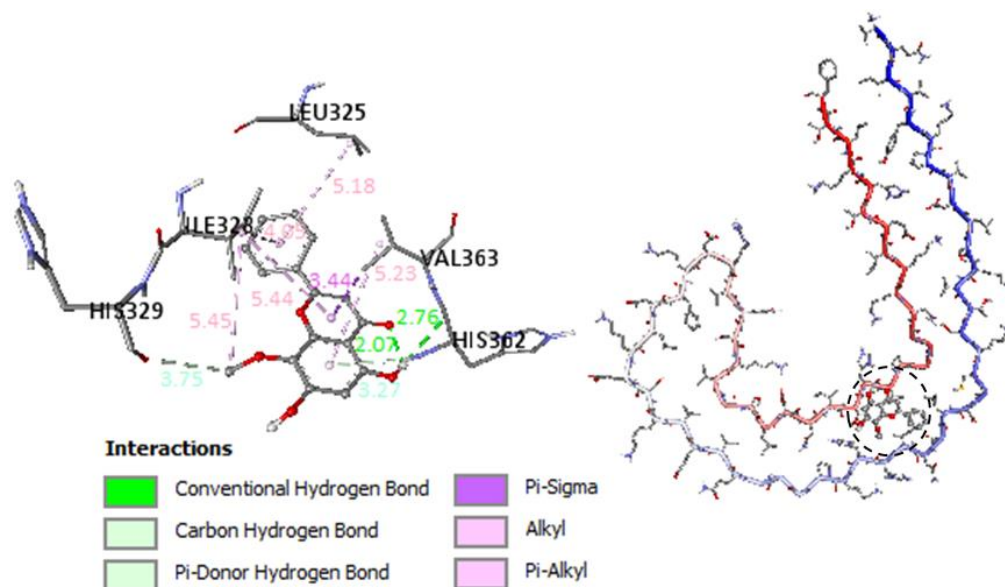


Figure 9. Wogonin docked into tau protein (right) and amino acid residues involved in the interaction (left) the dashed lines show the distance (in Å)

Molecular dynamic simulation of amyloid β

A 50-ns molecular dynamics simulation was carried out for $A\beta_{1-42}$ peptide in complex with selected natural polyphenols to examine the quality and stability of the modeled structures in the biological environment. The backbone atoms' root-mean-square deviation (RMSD) values during the MD simulation were obtained. This is a way to determine whether the system is stable or not. The 2D RMSD plots of the backbone C α atoms in $A\beta_{1-42}$ peptide and ligands fit on the protein were presented in Figures 10A, B, C, and D. In the case of chrysin, the RMSD value of the protein increased during the first 10ns due to the relaxation of the structure from the starting conformation and then was stabilized during the entire simulation time. The RMSD of chrysin fit on the $A\beta_{1-42}$ peptide exhibits a sharp increase in the first 3ns. Still, it reaches a plateau and becomes stable after about 22ns (Figure 10A). The RMSD of $A\beta_{1-42}$ peptide in complex with datiscetin attained stable equilibration after ~20ns. Figure 10B showed high values of datiscetin's deviation on the protein and did not stabilize during all 50ns, indicating an unstable

structure. As shown in Figure 10C, the RMSD of both $A\beta_{1-42}$ peptide and naringenin increased during the initial 10 ns of simulations and then tended to converge, indicating the system was stable and equilibrated. The RMSD of $A\beta_{1-42}$ peptide in complex with wogonin increased at about 15ns and then fluctuated with small oscillations indicating that the structure is equilibrated. As can be seen in Figure 10D, the structure of wogonin converged to a stable conformation after 35ns, which is evident from the convergence of RMSD.

The trajectory's residue-based root means square fluctuation (RMSF) was calculated to examine the flexibility of the peptide structure. Higher RMSF values show greater flexibility during the MD simulation. RMSF was calculated for amyloid β with 42 amino acids in complex with selected ligands. The RMSF trend appeared small and within the normal range (Figures 11A, B, C, and D). The average RMSF values were 0.47, 0.51, 0.56, and 0.54 nm for chrysin, datiscetin, naringenin, and wogonin, respectively, indicating a high degree of stability, corroborating the results obtained with the RMSD analysis.

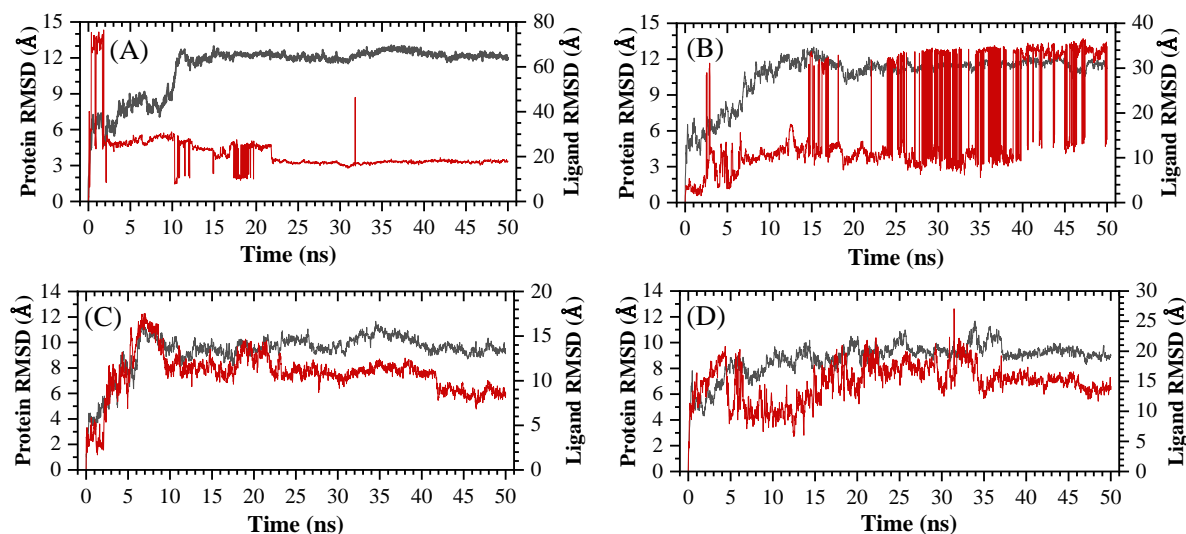


Figure 10. RMSD plots for the backbone C α atoms of the A β_{1-42} peptide (black) and A β_{1-42} peptide in complex with ligands (red). A) chrysin, B) datiscetin, C) naringenin, D) wogonin

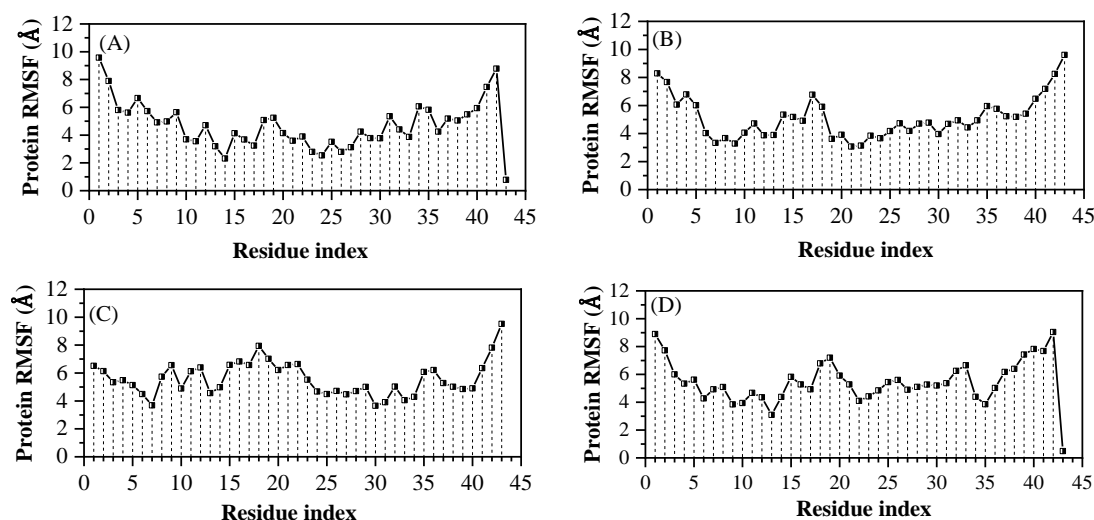


Figure 11. RMSF plots for the backbone C α atoms of the A β_{1-42} peptide in complex with chrysin (A), datiscetin (B), naringenin (C), and wogonin (D)

Figures 12A, B, C, and D summarize a timeline representation of the protein–ligand interactions and contacts.

According to Figure 12, many residues allow more than one direct interaction with the ligands. In detail, a higher percentage of hydrophobic interactions was observed in the A β_{1-42} complex with chrysin and wogonin due to their non-polar nature and fewer hydroxyl groups, while in naringenin and datiscetin with 1 and 2 more hydroxyl groups, respectively,

hydrogen bonds and water bridges play the most critical role in the ligand interaction with protein.

Schemes of detailed ligand atom interactions with amyloid β residues are presented (Figure 13).

During 66% of the simulation time oxygen atom of the carbonyl group in chrysin served as an acceptor of an intramolecular hydrogen bond from the nearest hydroxyl group. In contrast, oxygen of this hydroxyl group accepted hydrogen from Gly38, complemented by a water bridge.

Residues involved in hydrophobic interaction with chrysin are shown with green spheres around the ligand molecule, which are Phe19, Ile31, Ala2, Val36, Leu34, and Phe20 (Figure 13A). In amyloid β -datiscetin conjugate (Figure

13B) H atom of -OH group at position 2' served as a donor of H-bond interacting with His6, Leu34, and Met35 during 6, 19 and 16% of simulation time, respectively.

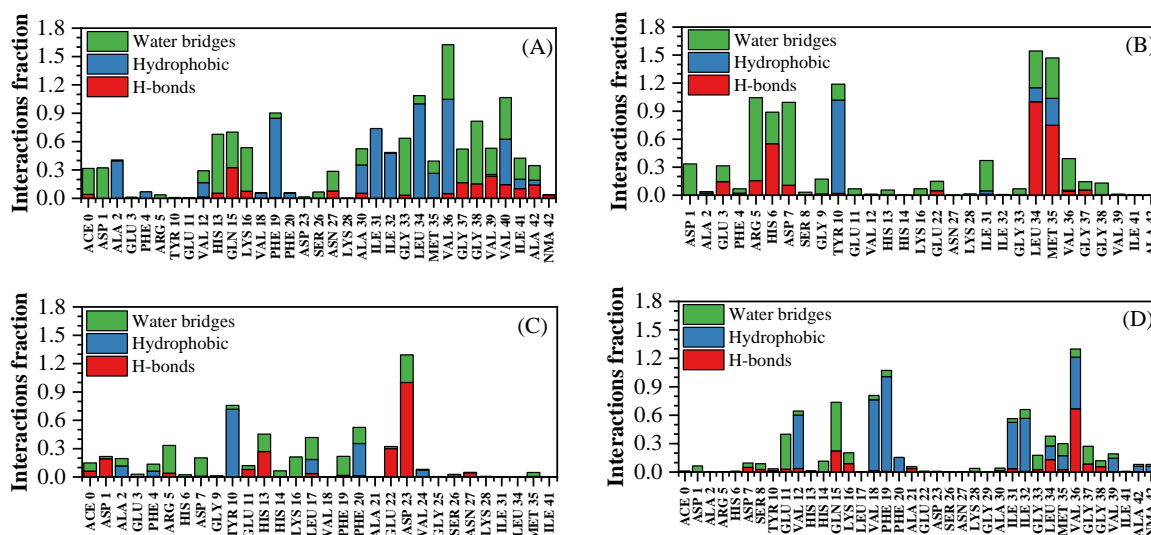


Figure 12. The bar charts of protein-ligand interaction fraction in course of simulation. A) chrysin, B) datiscetin, C) naringenin, D) wogonin

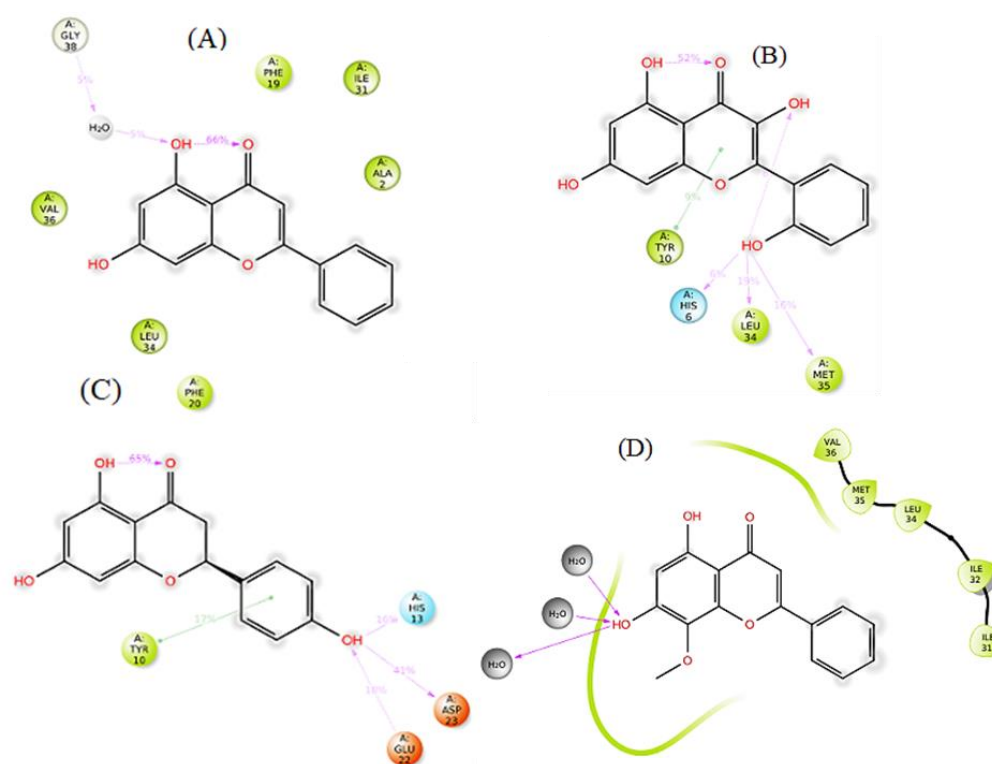


Figure 13. Residue interaction pattern of of the $A\beta_{1-42}$ peptide in complex with chrysin (A), datiscetin (B), naringenin (C), and wogonin (D)

Figure 13B shows ring C of datiscetin form π - π stacking with Tyr10 during 9% of a simulation time. Furthermore, two intramolecular hydrogen bonds are observed between -OH5 with carbonyl and two hydroxyl groups at positions 3 and 2'. The MD simulation results of naringenin show that hydroxyl groups at position 4' provide a hydrogen bond donor for His13 and Asp23 and a hydrogen bond acceptor for Glu22. The π - π stacking between Tyr10 and naringenin aromatic core is observed in 17% of the simulation time (Figure 13C). Figure 13D shows that wogonin is encapsulated inside the hydrophobic cavity of amyloid β , where it interacts with Val36, Met35, Leu4, Ile32 and Ile31. In addition, the hydroxyl

group at position 7 participates in hydrogen bonds with water molecules.

The secondary structure of amyloid β in complex with selected ligands at initiation and the end of the simulation are shown in Figure 14. There is a significant loss of α -helix content in all the systems considered with the formation of turns and random coils. The percentages of the secondary structures of A β_{42} observed (helix, coil, and turn) were calculated and plotted in Figure 15. As can be seen, the amyloid-wogonin system showed the maximum loss of α -helix structure, approximately 50%, and the largest percentage increase of about 70% in turn structure.

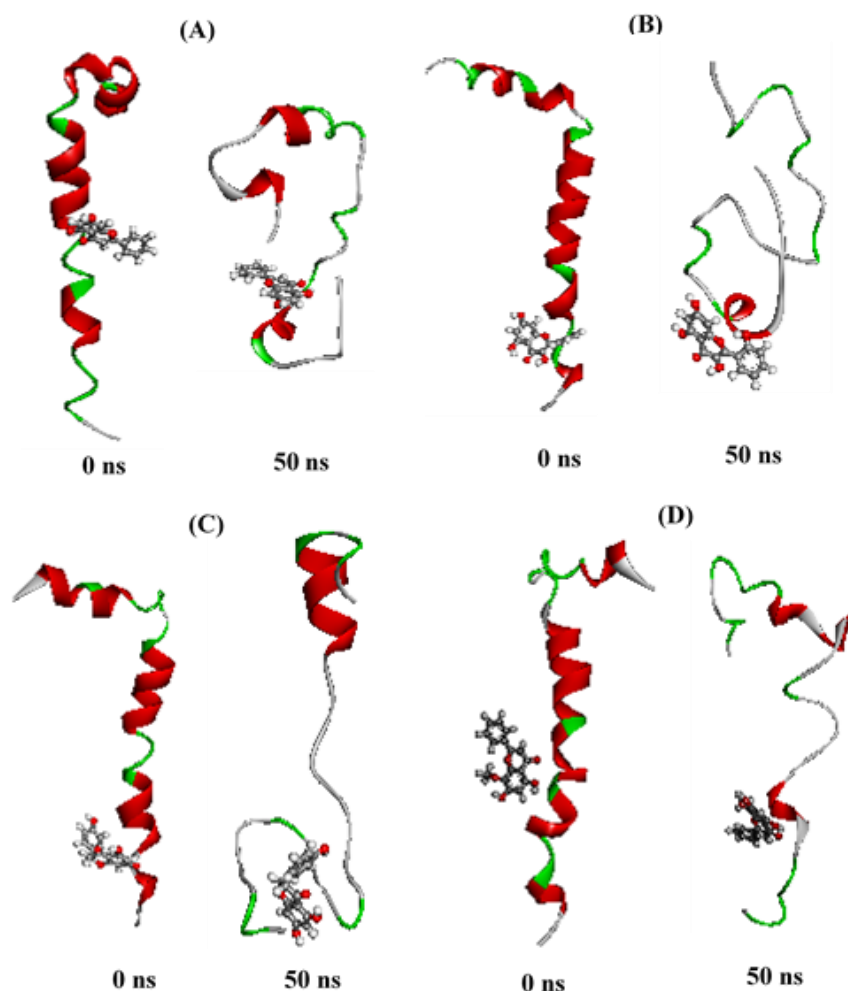


Figure 14. The secondary structure of amyloid β in complex with chrysin (A), datiscetin (B), naringenin (C), and wogonin (D) at 0 and 50ns

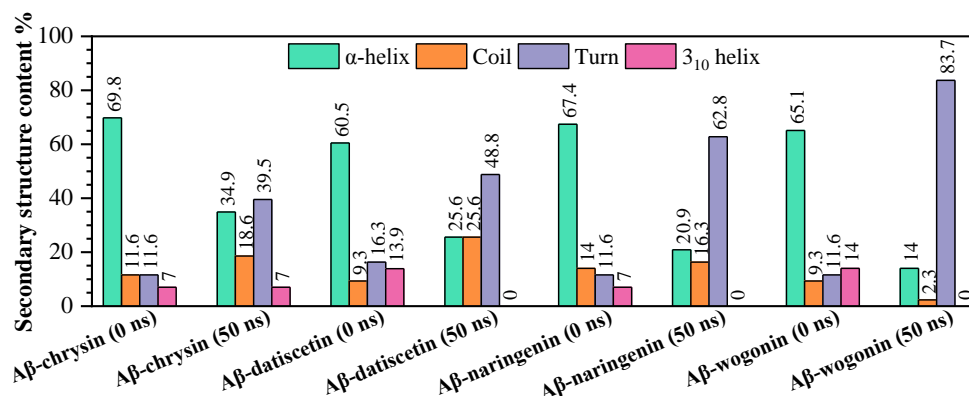


Figure 15. The percentages of the secondary structures of Aβ₁₋₄₂ in complex with selected ligands at 0 and 50ns

Molecular dynamic simulation of tau protein

Figure 16 gives the complete trajectories of the Cα RMSDs of tau protein in complex with selected ligands, and ligands fit on the protein.

The RMSD of tau protein in complex with chrysin was unstable up to 25ns, ranging from ~0.6 to ~1.5 nm, and stable at ~1.5 nm from 25 to 50ns. Chrysin fit on tau protein showed lower deviation, which slowly increased during the first ~15ns and stabilized throughout the simulation (Figure 16A). Figure 16B demonstrates an initial

increase in tau protein RMSD, reaching ~1.5 nm at around 10ns and then attaining significant stability. In contrast, the increase in RMSD of datiscetin fit on tau protein lasted up to 20ns and reached stability. High deviations were recorded in the initial ~10ns time interval for both tau protein and naringenin. Then RMSD values were found to be stable after ~25ns (Figure 16C). In the case of wogonin, the maximum increase in protein and ligand RMSD was observed in the first 15ns and continued with a slight slope until the end of the simulation (Figure 16D).

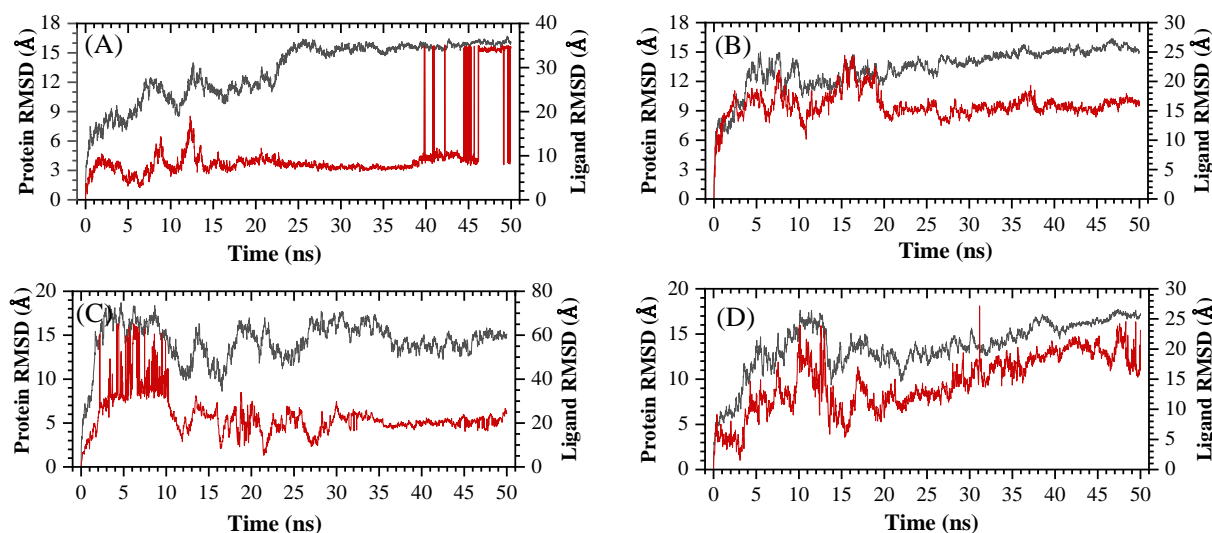


Figure 16. RMSD plots for the backbone Cα atoms of the tau protein (black) and in complex with ligands (red). A) chrysin, B) datiscetin, C) naringenin, D) wogonin

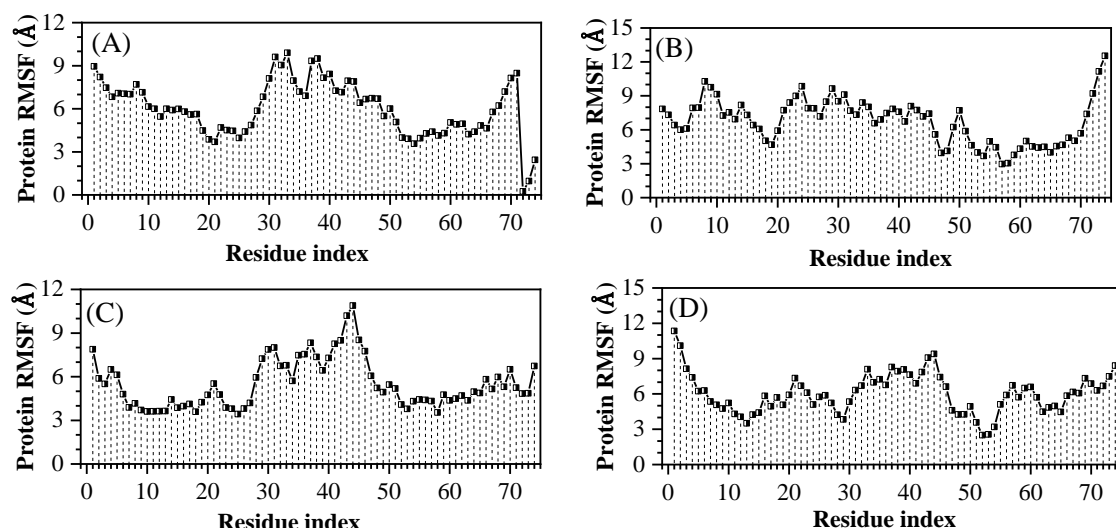


Figure 17. RMSF plots for the backbone C α atoms of the tau protein in complex with chrysin (A), datiscetin (B), naringenin (C), and wogonin (D)

To highlight the more flexible regions of tau protein in complex with selected ligands, the RMSF of the α -carbon positions averaged per residue was calculated and plotted in Figure 17. The results showed that all systems followed a similar fluctuation pattern, and the highest RMSF values were observed for the amino acids in the middle (residues from about 30 to 50). In contrast, the remaining amino acid residues recorded lower fluctuations.

The interaction fraction for the four candidate ligands is revealed in Figure 18. The results show

that many amino acids interact more than one type with the selected ligands. His330 made the most significant number of bridged hydrogen bonds, as well as direct hydrogen bond with $-C=O$ and $-OH5$ groups of chrysin (Figure 18A). A hydrophobic content is a prominent interaction with residues Ile328, Ile360, and Val363, whereas amino acids Ser320, Ser324, Thr361, and His362 form water bridges between tau protein and chrysin (Figure 18A).

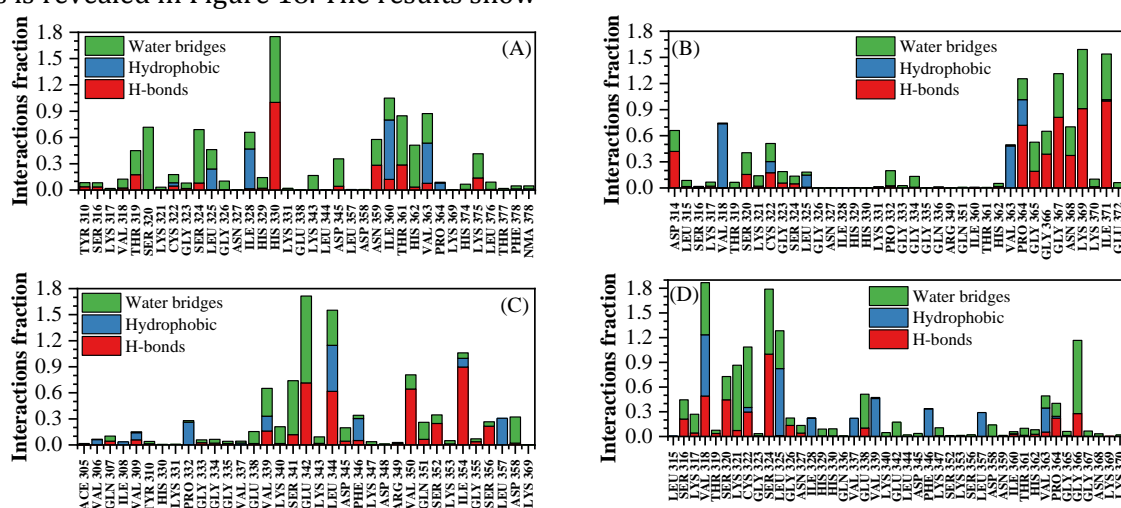


Figure 18. The bar charts of tau protein-ligand interaction fraction in course of simulation. A) chrysin, B) datiscetin, C) naringenin, D) wogonin

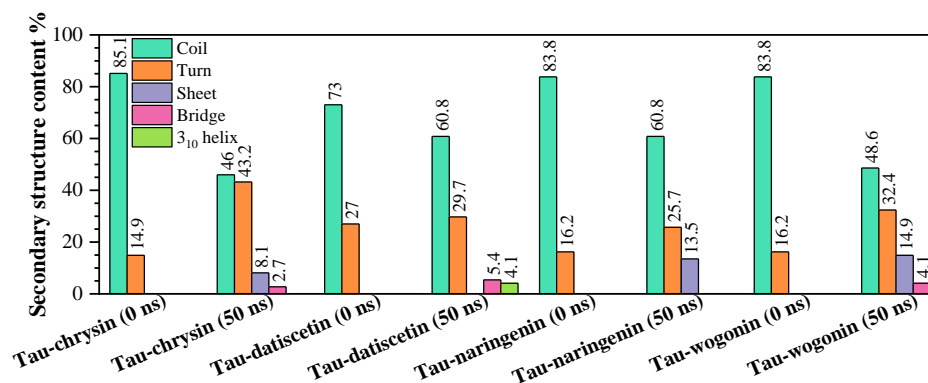


Figure 19. The percentages of the secondary structures of tau protein in complex with selected ligands at 0 and 50ns

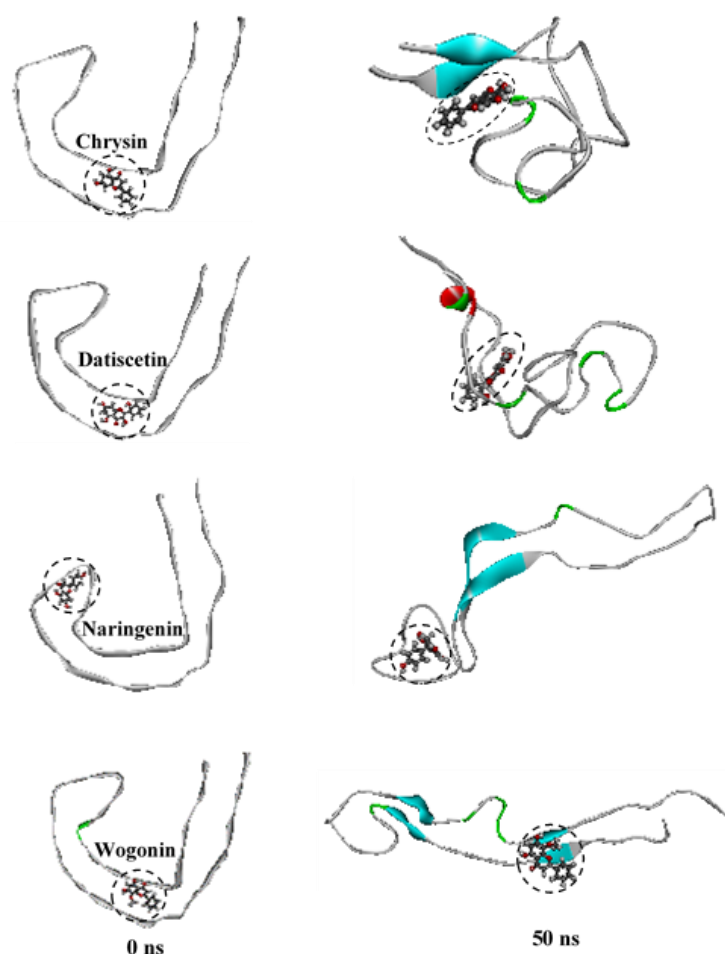


Figure 20. The secondary structure of tau protein in complex with chrysin (A), datiscetin (B), naringenin (C), and wogonin (D) at 0 and 50ns

The stacked bar charts (Figure 18B) exhibit that the residues Asp314, Pro364, Gly365, Gly366, Gly367, Asn368, Lys369, and Ile371 are

attributed to the largest number of water bridge and H-bond interactions with datiscetin during the simulation. Other residues which outline

hydrophobic contacts during MD simulation are Val318 and Val363. Naringenin interacted with the protein backbone by forming bridged and direct hydrogen bonding interactions with Val339, Ser341, Glu342, Ile344, Val 350, and Ile354 residues. In addition, hydrophobic interactions are exhibited involving residues Val339 and Ile344 (Figure 18C). Wogonin develops bridge and direct hydrogen bonds with Val318, Ser320, Lys321, Cys322, Ser324, and Gly366. A hydrophobic interaction is also formed with Val318 and Leu325 (Figure 18D).

The secondary structure analyses of tau protein versus the simulation time are shown in Figures 19 and 20. In all systems, the coil percentage dropped off within 50ns, whereas the turn percentage increased. The tau-chrysin and tau-datiscetin systems showed the maximum and minimum loss of coil structure, respectively. Also, these two systems showed the highest and lowest increase in the percentage of turn protein secondary structure, respectively. Except for the tau-datiscetin system, short β -sheets appeared in three other systems. Conversely, transient 3_{10} helices were observed just in the tau-datiscetin system.

Conclusions

Herein, we provided structural insights into some natural flavonoid mechanisms for inhibiting A β and tau protein aggregation involved in AD pathology. Based on molecular docking results, the structural difference between these compounds, due to the number and position of hydroxyl groups in the B and C rings, did not significantly affect their binding constant to the receptors. In contrast, the difference in the binding mechanism resulted from interaction with different amino acids via different forces. Chrysin and datiscetin, with a similar binding energy of -5.5 kcal/mol, showed slightly higher efficiency in binding to A β than naringenin and wogonin (binding energy of -5.4

kcal/mol), which was due to more interaction with residues at the binding site. The results confirmed that many amino acids interact more than one type with the selected ligands. Because of their non-polar nature and fewer hydroxyl groups, the A β complex with chrysin and wogonin has a higher percentage of hydrophobic interactions, whereas in naringenin and datiscetin, which have hydroxyl groups in rings B and C, hydrogen bonds and water bridges play an essential role in the interaction process. Structural changes in amyloid β in the presence of all four compounds were seen as a decrease in α -helix content and an increase in the percentage of turns and random coils, which was the most for wogonin-A β conjugate. The tau binding free energy is in the order of naringenin > datiscetin > wogonin > chrysin with slight differences (from -5.9 kcal/mol to -5.5 kcal/mol). The highest binding affinity of naringenin for tau protein was found due to its different binding site and interaction with Phe364, Leu344, and Val350 residues. While hydrogen bonds and water bridges are specific in stabilizing tau conjugate with naringenin and datiscetin, hydrophobic contacts and hydrogen bonds with water are mainly involved in wogonin and chrysin complexes with tau protein. The secondary structure analysis results showed that the coil percentage decreases in all tau-ligand systems. In contrast, the turn percentage increases, with the highest in chrysin and the lowest in the presence of datiscetin. Also, short β -sheets appeared at tau-ligand complexes except for datiscetin. The results show that the introduced compounds can inhibit the aggregation of both amyloid beta and tau protein and can be used as promising candidates for treating Alzheimer's disease.

Acknowledgment


We sincerely thank Dr. Farshad Shiri for his assistance and for performing the molecular dynamic simulation.

Disclosure statement

The authors declare that they have no conflict of interest.

Orcid

Saba Hadidi : [0000-0003-1446-1265](https://orcid.org/0000-0003-1446-1265)

Mohammad Hosein Farzaei : [0000-0001-7081-6521](https://orcid.org/0000-0001-7081-6521)

References

- [1] M.G. Ulep, S.K. Saraon, S. McLea, Alzheimer disease, *J. Nurse Pract.*, **2018**, *14*, 129–135. [[CrossRef](#)], [[Google Scholar](#)], [[Publisher](#)]
- [2] A.S. Schachter, K.L. Davis, Alzheimer's disease, *Dialogues Clin. Neurosci.*, **2022**, *2*, 91–100. [[CrossRef](#)], [[Google Scholar](#)], [[Publisher](#)]
- [3] S. Choi, W.J. Jahng, S.M. Park, D. Jee, *Am. J. Ophthalmol.*, **2020**, *210*, 41–47. [[CrossRef](#)], [[Google Scholar](#)], [[Publisher](#)]
- [4] Z. Breijyeh, R. Karaman, *Molecules*, **2020**, *25*, 5789. [[CrossRef](#)], [[Google Scholar](#)], [[Publisher](#)]
- [5] T. Pardo-Moreno, A. González-Acedo, A. Rivas-Domínguez, V. García-Morales, F.J. García-Cozar, J.J. Ramos-Rodríguez, L. Melguizo-Rodríguez, *Pharmaceutics*, **2022**, *14*, 1117. [[CrossRef](#)], [[Google Scholar](#)], [[Publisher](#)]
- [6] M.H. Murdock, L.-H. Tsai, *Nat. Neurosci.*, **2023**, 1–15. [[CrossRef](#)], [[Google Scholar](#)], [[Publisher](#)]
- [7] Y. Matsuzaka, R. Yashiro, *Biologics*, **2023**, *3*, 23–39. [[CrossRef](#)], [[Google Scholar](#)], [[Publisher](#)]
- [8] M. Raju, V.P. Gopi, V. Anitha, K.A. Wahid, *Phys. Eng. Sci. Med.*, **2020**, *43*, 1219–1228. [[CrossRef](#)], [[Google Scholar](#)], [[Publisher](#)]
- [9] P.A. Chawla, V. Parikh, *CNS Neurol Disord Drug Targets*, **2020**, *19*, 646–647. [[CrossRef](#)], [[Google Scholar](#)], [[Publisher](#)]
- [10] A. De Simone, M. Naldi, D. Tedesco, M. Bartolini, L. Davani, V. Andrisano, *J. Pharm. Biomed. Anal.*, **2020**, *178*, 112899. [[CrossRef](#)], [[Google Scholar](#)], [[Publisher](#)]
- [11] J.F. González, A.R. Alcántara, A.L. Doadrio, J.M. Sánchez-Montero, *Expert Opin. Drug Discov.*, **2019**, *14*, 879–891. [[CrossRef](#)], [[Google Scholar](#)], [[Publisher](#)]
- [12] Y. Ju, K.Y. Tam, *Neural Regen. Res.*, **2022**, *17*, 543–549. [[CrossRef](#)], [[Google Scholar](#)], [[Publisher](#)]
- [13] S. Manchanda, L. Galan-Acosta, A. Abelein, S. Tambaro, G. Chen, P. Nilsson, J. Johansson, *Mol. Ther.*, **2023**, *31*, 487–502. [[CrossRef](#)], [[Google Scholar](#)], [[Publisher](#)]
- [14] N.A. Althobaiti, F. Menaa, J.J. Dalzell, B.D. Green, *Neural Regen. Res.*, **2023**, *18*, 113–114. [[CrossRef](#)], [[Google Scholar](#)], [[Publisher](#)]
- [15] V.H. Finder, R. Glockshuber, *Neurodegener. Dis.*, **2007**, *4*, 13–27. [[CrossRef](#)], [[Google Scholar](#)], [[Publisher](#)]
- [16] A. Takashima, *Curr. Alzheimer Res.*, **2010**, *7*, 665–669. [[CrossRef](#)], [[Google Scholar](#)], [[Publisher](#)]
- [17] C.M. Wischik, C.R. Harrington, J.M. Storey, *Biochem. Pharmacol.*, **2014**, *88*, 529–539. [[CrossRef](#)], [[Google Scholar](#)], [[Publisher](#)]
- [18] H. Ashrafian, E.H. Zadeh, R.H. Khan, *Int. J. Biol. Macromol.*, **2021**, *167*, 382–394. [[CrossRef](#)], [[Google Scholar](#)], [[Publisher](#)]
- [19] N. Job, V.S. Thimmakondur, K. Thirumoorthy, *Molecules*, **2023**, *28*, 1388. [[CrossRef](#)], [[Google Scholar](#)], [[Publisher](#)]
- [20] F.I. Baptista, A.G. Henriques, A.M. Silva, J. Wiltfang, O.A. da Cruz e Silva, *ACS Chem. Neurosci.*, **2014**, *5*, 83–92. [[CrossRef](#)], [[Google Scholar](#)], [[Publisher](#)]
- [21] M. Uddin, M. Kabir, K. Niaz, P. Jeandet, C. Clément, B. Mathew, A. Rauf, K.R. Rengasamy, E. Sobarzo-Sánchez, G.M. Ashraf, *Molecules*, **2020**, *25*, 1267. [[CrossRef](#)], [[Google Scholar](#)], [[Publisher](#)]
- [22] Y. Wen, L. Zhang, N. Li, A. Tong, C. Zhao, *Food Frontiers*, **2023**, 1–17. [[CrossRef](#)], [[Google Scholar](#)], [[Publisher](#)]
- [23] Y. Zhu, J. Wang, *Neurol. Sci.*, **2015**, *36*, 1181–1188. [[CrossRef](#)], [[Google Scholar](#)], [[Publisher](#)]

- [24] S. Ghofrani, M.-T. Joghataei, S. Mohseni, T. Baluchnejadmojarad, M. Bagheri, S. Khamse, M. Roghani, *Eur. J. Pharmacol.*, **2015**, 764, 195–201. [[CrossRef](#)], [[Google Scholar](#)], [[Publisher](#)]
- [25] M. Hanaki, K. Murakami, K.I. Akagi, K. Irie, *Bioorg. Med. Chem.*, **2016**, 24, 304–313. [[CrossRef](#)], [[Google Scholar](#)], [[Publisher](#)]
- [26] A. Vedagiri, S. Thangarajan, *Neuropeptides*, **2016**, 58, 111–125. [[CrossRef](#)], [[Google Scholar](#)], [[Publisher](#)]
- [27] H. Zeng, X. Wu, *Eur. J. Med. Chem.*, **2016**, 121, 851–863. [[CrossRef](#)], [[Google Scholar](#)], [[Publisher](#)]
- [28] M.D. Paranjpe, A. Taubes, M. Sirota, *Trends Pharmacol. Sci.*, **2019**, 40, 565–576. [[CrossRef](#)], [[Google Scholar](#)], [[Publisher](#)]
- [29] M. Awasthi, S. Singh, S. Tiwari, V.P. Pandey, U.N. Dwivedi, **2018**, 483–511. [[CrossRef](#)], [[Google Scholar](#)], [[Publisher](#)]
- [30] H.E. Pence, A. Williams, *ChemSpider: an online chemical information resource*, ACS Publications, **2010**. [[CrossRef](#)], [[Google Scholar](#)], [[Publisher](#)]
- [31] H.M. Berman, J. Westbrook, Z. Feng, G. Gilliland, T.N. Bhat, H. Weissig, I.N. Shindyalov, P.E. Bourne, *Nucleic Acids Res.*, **2000**, 28, 235–242. [[CrossRef](#)], [[Google Scholar](#)], [[Publisher](#)]
- [32] O. Crescenzi, S. Tomaselli, R. Guerrini, S. Salvadori, A.M. D'Ursi, P.A. Temussi, D. Picone, *Eur. J. Biochem.*, **2002**, 269, 5642–5648. [[CrossRef](#)], [[Google Scholar](#)], [[Publisher](#)]
- [33] O. Trott, A.J. Olson, *J. Comput. Chem.*, **2010**, 31, 455–461. [[CrossRef](#)], [[Google Scholar](#)], [[Publisher](#)]
- [34] K.J. Bowers, D.E. Chow, H. Xu, R.O. Dror, M.P. Eastwood, B.A. Gregersen, J.L. Klepeis, I. Kolossvary, M.A. Moraes, F.D. Sacerdoti, IEEE, **2006**, 43–43. [[CrossRef](#)], [[Google Scholar](#)], [[Publisher](#)]
- [35] N. Shahabadi, F. Shiri, R. Khodarahmi, *J. Mol. Liq.*, **2022**, 345, 117904. [[CrossRef](#)], [[Google Scholar](#)], [[Publisher](#)]
- [36] J. Zielkiewicz, Structural properties of water: *J. Chem. Phys.*, **2005**, 123, 104501. [[CrossRef](#)], [[Google Scholar](#)], [[Publisher](#)]
- [37] G.J. Martyna, M.L. Klein, M. Tuckerman, *J. Chem. Phys.*, **1992**, 97, 2635–2643. [[CrossRef](#)], [[Google Scholar](#)], [[Publisher](#)]
- [38] J.L. Banks, H.S. Beard, Y. Cao, A.E. Cho, W. Damm, R. Farid, A.K. Felts, T.A. Halgren, D.T. Mainz, J.R. Maple, *J. Comput. Chem.*, **2005**, 26, 1752–1780. [[CrossRef](#)], [[Google Scholar](#)], [[Publisher](#)]
- [39] W. Humphrey, A. Dalke, K. Schulten, *J. Mol. Graph.*, **1996**, 14, 33–38. [[CrossRef](#)], [[Google Scholar](#)], [[Publisher](#)]
- [40] H. Onoda, O. Shoji, K. Suzuki, H. Sugimoto, Y. Shiro, Y. Watanabe, *Catal. Sci. Technol.*, **2018**, 8, 434–442. [[CrossRef](#)], [[Google Scholar](#)], [[Publisher](#)]
- [41] M. Sato, K. Murakami, M. Uno, Y. Nakagawa, S. Katayama, K.I. Akagi, Y. Masuda, K. Takegoshi, K. Irie, *J. Biol. Chem.*, **2013**, 288, 23212–23224. [[CrossRef](#)], [[Google Scholar](#)], [[Publisher](#)]
- [42] A. Yang, C. Liu, H. Zhang, J. Wu, R. Shen, X. Kou, *Eur. J. Med. Chem.*, **2022**, 233, 114216. [[CrossRef](#)], [[Google Scholar](#)], [[Publisher](#)]
- [43] H. Shi, B. Kang, J.Y. Lee, *J. Phys. Chem. B.*, **2016**, 120, 11405–11411. [[CrossRef](#)], [[Google Scholar](#)], [[Publisher](#)]

HOW TO CITE THIS ARTICLE

Saba Hadidi *, Mohammad Hosein Farzaei. Inhibitory Activity of Natural Flavonoids against Protein Aggregation in Alzheimer's disease: A Computational Simulation Study. *Adv. J. Chem. A*, **2023**, 6(2), 123-140.

DOI: [10.22034/AJCA.2023.379103.1350](https://doi.org/10.22034/AJCA.2023.379103.1350)

URL: http://www.ajchem-a.com/article_167687.html